Silicon Carbide Preforms for Metal Infiltration by Selective Laser Sintering™ of Polymer Encapsulated Powders

N.K. Vail†, J.W. Barlow†, and H.L. Marcus‡
†. Department of Chemical Engineering
‡. Center for Materials Science and Engineering
The University of Texas at Austin

Abstract

A polymer encapsulated silicon carbide system has been developed for use with Selective Laser Sintering. Extensive studies with this material have provided information pertaining to processing and material parameters which most affect the strengths and densities of resulting green parts. The important parameters considered were particle size distribution of the powders, laser scanning conditions, and laser beam diameter. Simple and complex shapes were easily produced with this material using optimized parameters. Green objects were infused with metal by Lanxide using their pressureless infiltration process to produce both metal matrix and ceramic matrix composites.
(Key Words: Silicon Carbide, Encapsulation, Polymer, Selective Laser Sintering, Composites).

Introduction

Polymer encapsulated, high temperature powder material systems for Selective Laser Sintering have been under development at The University of Texas for the past few years[1,2]. These materials offer a convenient path to complex ceramic and metal preforms via SLS. Several systems, including glass[3], alumina and silica-zircon[4], and copper[2], have been demonstrated to be viable materials for the fabrication of preforms.

Recent work has focused on investigating possible applications for the material systems under development. Additionally, it is desired to compare the performance of SLS preforms against that of other, more conventional preform manufacturing methods during post-processing steps. To this end, a polymer encapsulated silicon carbide system has been developed to produce preforms for use with Lanxide's pressureless infiltration process[5,6,7]. The results of the infiltration will be described in a separate paper in this symposium.

Materials and Methods

Four particle size distributions of silicon carbide were provided by Lanxide Corporation. These powders were designated L-1000, L-800, L-500, and L-220, according to their specified grit sizes. Figure 1 shows the particle size distributions of these powders as measured by a

Coulter Multisizer. A poly(methylmethacrylate) latex polymer was produced as described elsewhere[8]. This polymer was formulated to have a specified melt flow index (ASTM D1238) of 30 g/10 min as measured using a Kayness Galaxy I capillary rheometer at conditions of 200°C and 75 psi. The polymer had an actual melt flow index of 32.2 g/10min. The glass transition temperature, T_g, of the polymer was determined to be 105°C using Differential Scanning Calorimetry.

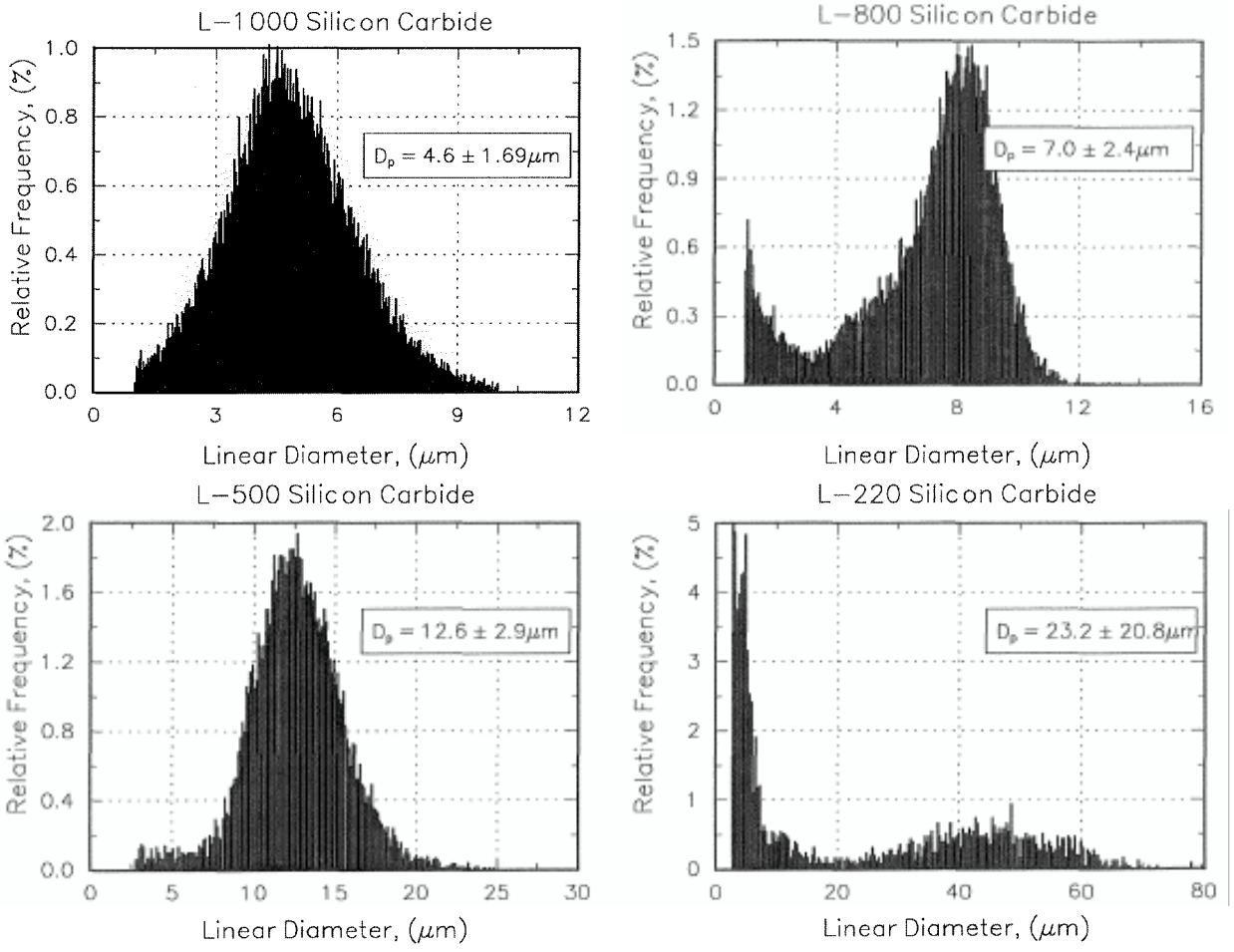

Figure 1. Particle size distributions of silicon carbide powders.

Two batches of polymer encapsulated silicon carbide, each consisting of a different particle size distribution, were prepared by spray drying according to methods described previously[1]. The drying conditions were maintained to yield an agglomerated particle morphology. The initial batch was encapsulated to obtain a polymer composition of 30 vol. % (13.8 wt. %). The second batch was encapsulated to obtain a polymer composition of 25 vol. % (11.1 wt. %). The resulting encapsulated powders were admixed with pure silicon carbide powder to reduce the polymer content to 20 vol. % (8.5 wt. %). It has been shown that mixtures

of encapsulated powders with pure materials increases the apparent packing density of the powder[3]. Polymer compositions of all powders were determined by Thermal Gravimetric Analysis (TGA). Figure 2 shows an electron micrograph of the initial batch of polymer encapsulated silicon carbide.

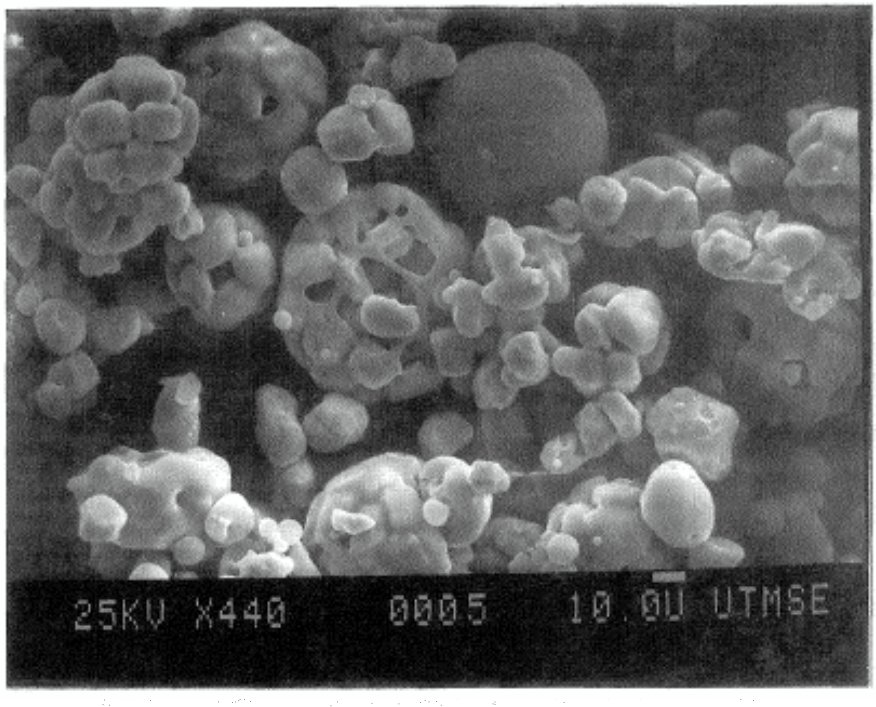

Figure 2. Polymer encapsulated L-500 silicon carbide powder prior to admixing of pure silicon carbide L-500.

The initial samples were prepared from a single particle size distribution consisting of the L-500 powder. The second set of samples used a quadmodal particle size distribution composed of all four supplied powder sizes according to the composition shown in Table 1. Figure 3 shows the particle size distribution for the premixed quadmodal powder as supplied by Lanxide Corp. This distribution was verified using a mixture of the component powders.

Table 1. Quadmodal distribution powder composition.

Powder	Amount, (wt. %)
L-220	47.0
L-500	25.0
L-800	16.0
L-1000	11.0

Selective Laser Sintering of Materials

Both batches of materials were processed at the DTM Corp. using an SLS™ Model 125

workstation equipped with a calibrated 25 watt CO_2 laser. The laser beam profile and diameter were determined using a beam profilometer. Processing was conducted in a nitrogen environment, less than 2% O_2, with a gas flow rate produced by a pressure differential of 0.04 in. H_2O. Surface bed temperatures were maintained at 119°C as determined by a infrared sensor using an emissivity, ε, of 0.90.

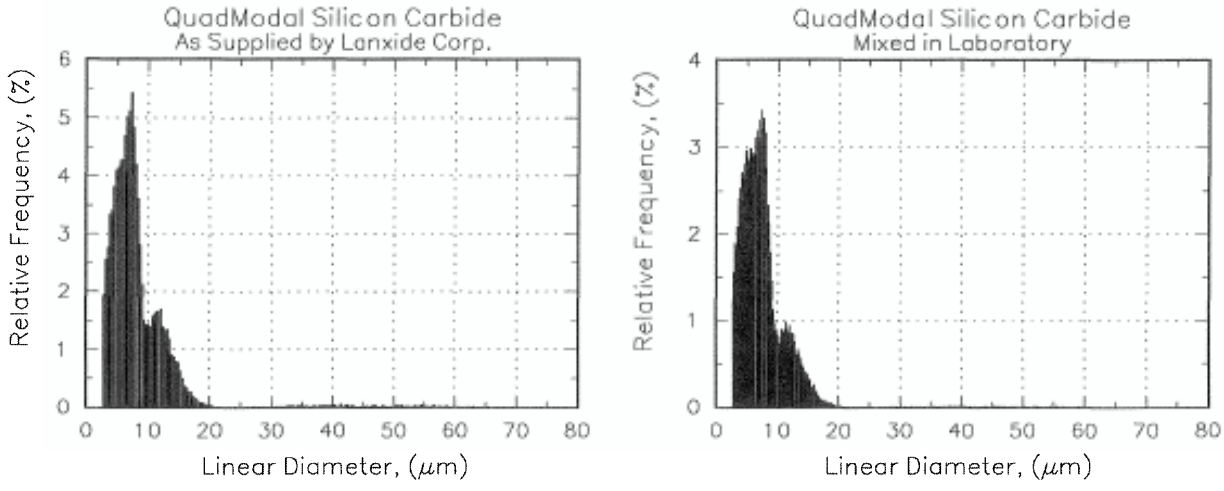

Figure 3. QuadModal particle size distribution.

Table 2 lists SLS operating parameters for the materials studied. 2"x2"x0.3" coupons for metal infiltration tests and 1"x3"x¼" coupons for characterization of green part properties were produced using the full range of SLS operating parameters. Complex shapes consisting of a thin walled electronical packaging box and an engine cowling were produced using optimized SLS operating parameters.

Table 2. Range of Selective Laser Sintering operating conditions.

Laser Power, (W)	Scan Speed, (ips)	Beam Spacing, (mils)	Layer Thickness, (mil)
6 - 16	50 - 100	2 - 5	4.5

Characterization of SLS Parts

Powder bed densities were measured using the method of density cups. Cups having a wall thickness of 3/16" and a volume 1.5" in diameter by 1" depth are produced by SLS using optimized operating parameters. Bed density is determined from the contained volume of powder. Cups are made at different bed locations to observe positional density variance. Part densities were determined from volume and mass measurements. Part green strengths were measured by three point bend analysis. Fracture planes of the bend specimens were examined by Scanning Electron Microscopy (SEM). Polymer content of the green parts were measured by TGA.

Results and Discussion

Monodistribution Powder

Initial experiments with this material were concerned with determining the effects of laser power, laser scan speed, and beam spacing on the strength and density of green parts. Nelson has shown, however, that these three critical SLS parameters are coupled and it is better to consider them as such when examining their influence on properties of objects produced by SLS[9]. Starting from scanning geometry and laser beam characteristics, Nelson derived the following expression for the laser power density

$$A_N = \frac{k' P}{BS * SCSP} \tag{1}$$

where A_N is the Andrew Number typically expressed in cal/cm^2, k' is a geometry specific constant, P is the laser power, BS is the beam speed, and SCSP is the scan spacing. Eq. (1) provides a convenient means of lumping the major SLS parameters and can be used to correlate green part properties such as strength and density. Furthermore, from Eq. (1), it follows that similar part properties may result for constant A_N with varying combinations of laser power, beam speed, and scan spacing.

Table 3. Effect of laser scanning parameters on part properties.

A_N, (cal/cm^2)	Laser Power, (W)	Scan Spacing, (mil)	Scan Speed, (ips)	Density, (g/cm^3)	Green Strength, (psi)
0.41	7	5	125	1.35	9.1
0.47	8	5	125	1.37	12.1
0.74	8	4	100	1.37	76.1
0.79	8	3	125	1.38	73.4
0.79	8	5	75	1.40	72.4
1.32	8	5	75	1.40	183.2
1.35	12	3	110	1.37	170.3
1.74	13	3	92	1.33	186.0
1.74	12	4	64	1.35	186.4
1.74	12	3	85	1.32	192.9
2.27	14	3	76	1.35	205.2
2.28	12	3	65	1.34	205.8

Table 3 shows the influence of fixed power densities, A_N, with varying laser power, beam speed, and scan spacing on resultant densities and strengths of three point bend specimens. The data clearly show green strength to be related to the power density and not to be influenced

significantly by the respective operating parameters. The data also show green strength to increase with A_N. As energy input is increased it is expected that sintering of polymer binder within the layer would increase as would the likelihood of fusing the layer to previous layers, thus, increasing green strength. At the point where interlayer bonding is achieved further increases in power density would no longer be expected to improve green density. In fact, further increases in power density would cause degradation of the polymer binder reducing green strength.

Figure 4 shows the influence of the scan density, A_N, on green strength. The trend is as suggested although no decrease in green strength is observed for the range of energy densities studied. A transition in green strength occurs at about A_N = 1.20 cal/cm^2 where the rate of strength increase diminishes to roughly 20% of the previous rate of strength development. Figure 5 and Figure 5 are SEM micrographs of green part fracture planes. In Figure 5, where $A_N < 1.2$, the layered structure of the part is very noticeable, whereas in Figure 5, where $A_N > 1.2$, the layered structure is noticeably absent.

Changes in the rate of strength development with energy input may be further attributed to changes in part density and thermal degradation of the polymer binder. Figure 8 shows density of the green parts to increase in manner similar to that of green strength. Increases in density are known to cause increases in material strength[10,11]. Figure 7 shows the effect of power density on the polymer content. The polymer volume content decreases nearly 15% over the range of A_N studied. This binder loss combined with power density saturation may contribute to the decrease of green strength development shown in Figure 4.

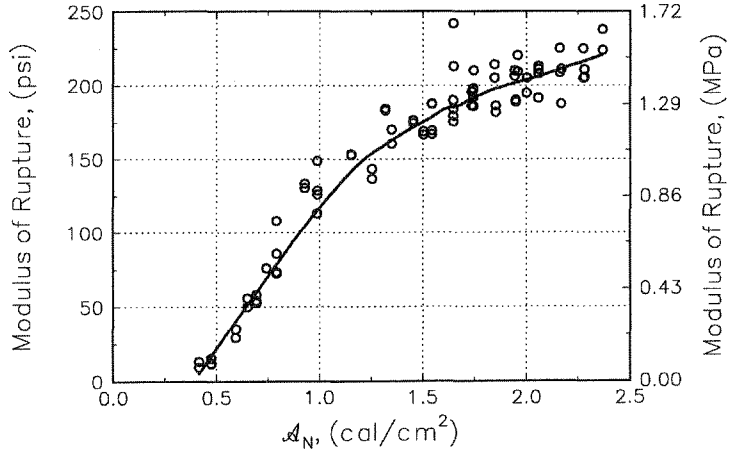

Figure 4. Influence of scan density on green strength.

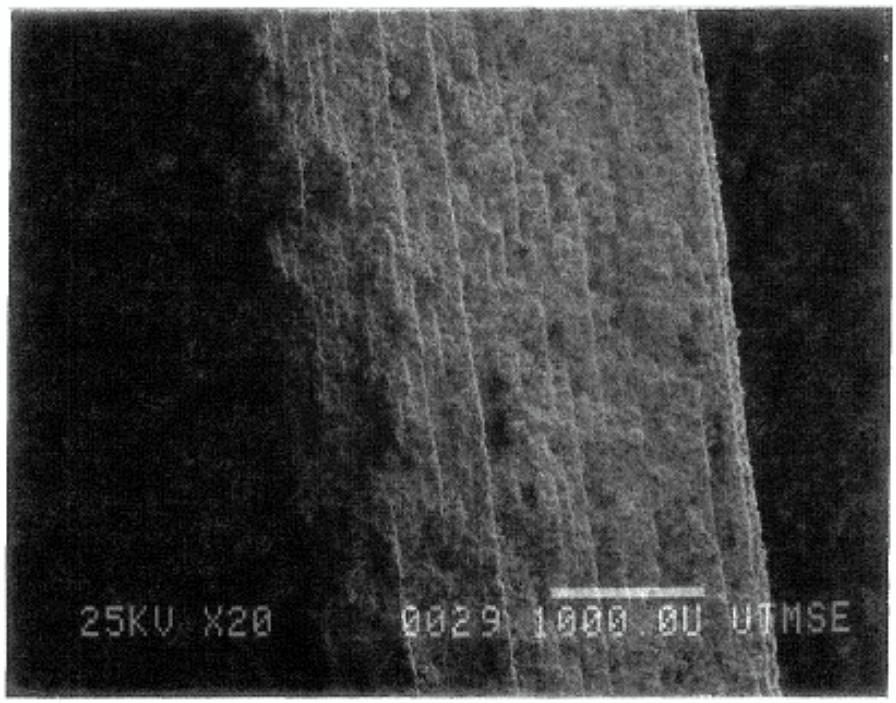

Figure 5. Poor interlayer bonding. A_N = 0.69 cal/cm^2. Scan conditions: 7W, 75 ips, and 3 mil beam spacing.

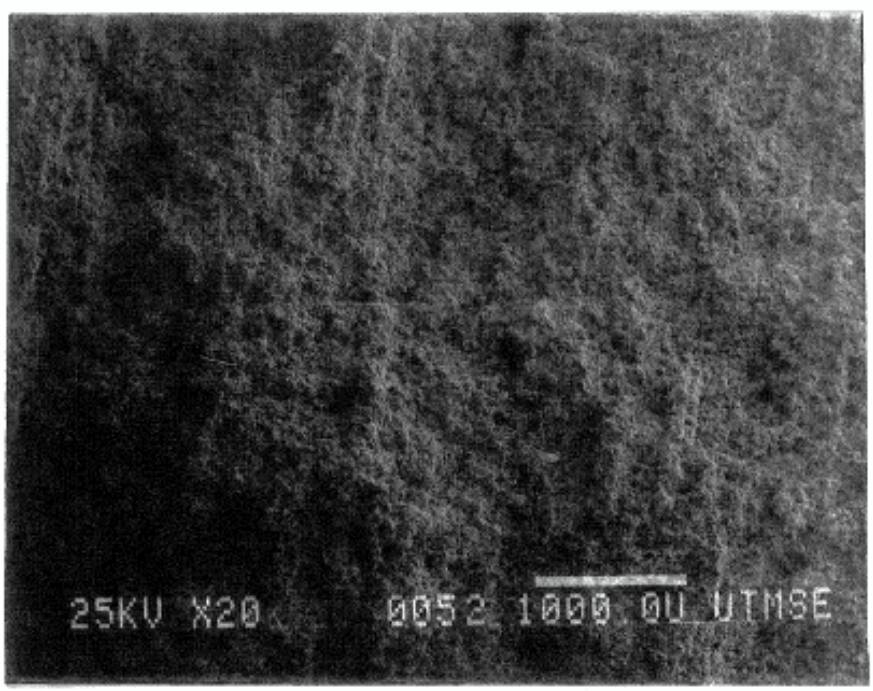

Figure 6. Good interlayer bonding. A_N = 2.00 cal/cm^2. Scanning conditions: 12W, 74 ips, and 3 mil beam spacing.

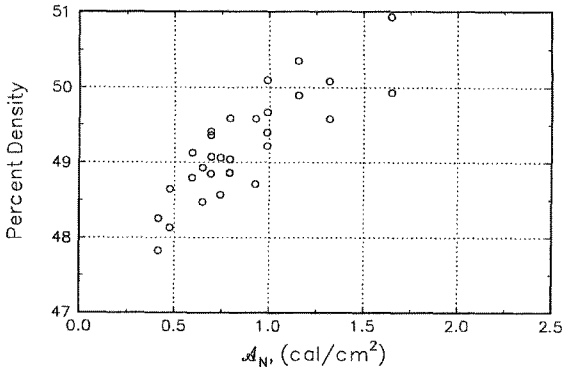

Figure 7. Influence of scan density on green density.

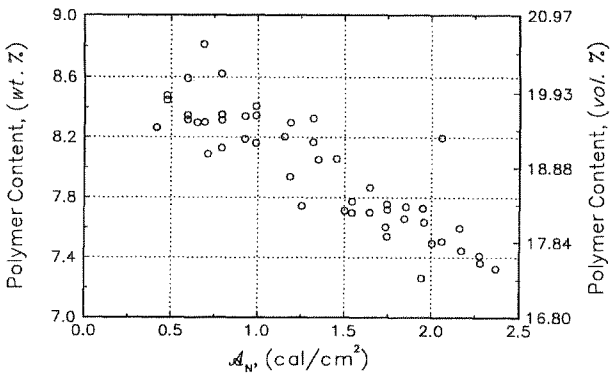

Figure 8. Effect of scan density on polymer content of green parts.

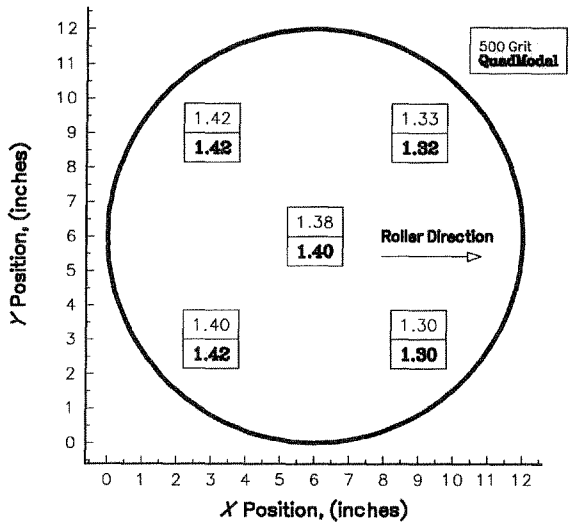

Figure 9. Influence bed position on powder bed density.

QuadModal Distribution Powder

This material, without binder, has an apparent tapped density of 62% compared to 52% for that of the L-500 powder. Therefore, it was hoped the quadmodal distribution material would improve green part density thereby increasing ceramic loading of the part. In practice, however, green densities were unchanged, still ranging from 48 to 51% as observed for the L-500 material. Tapped densities of the encapsulated powders were determined to be 57% and 59% for the quadmodal and L-500, respectively. Figure 9 shows the powder bed densities to be lower than the tapped densities, 46% (1.30 g/cm^3) to 50% (1.42 g/cm^3), and to decrease in the direction of the roller. This problem does not occur in the SLS Sinterstation™ 2000, the commercial machine, since the roller spreads powder in both directions[12]. Density changes across the bed are evident in the green parts, too.

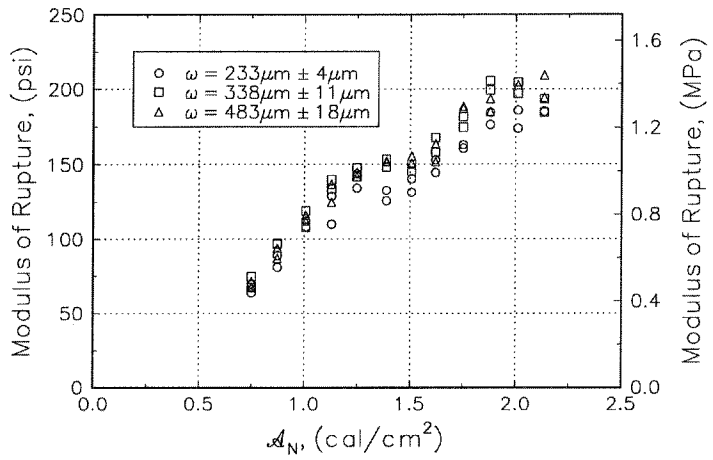

Figure 10. Effect of laser power density on strength of Quadmodal powder preforms.

Figure 10 shows the strength of green parts to develop with increasing Andrew Number, A_N, in a manner similar to the L-500 material. Additionally, the influence of laser beam diameter was investigated with this material. For the range of beam diameters studied, it can be seen that no appreciable effect on part strength is observed.

Conclusions and Further Work

The polymer encapsulated powders studied here were found to produce green shapes with good strength, surface finish, and dimensional accuracy. Figure 11 shows complex preforms produced from these materials. A broad range of SLS scanning conditions were determined suitable for producing parts with green strengths sufficient for processing by Lanxide Corporation. Typically, parts with green strengths greater than 125 psi (A_N > 1.0 cal/cm^2) were preferred since delamination was not observed during the infiltration process.

The quadmodal distribution powders did not perform as expected and further work is required to explain this result. It is possible the distribution is adversely effected by the encapsulation process. If this is indeed true, it may be advisable to encapsulate a one or more of the individual size fractions and then mix these with other individual size fractions to achieve a high packing material, thus, increasing the ceramic loading.

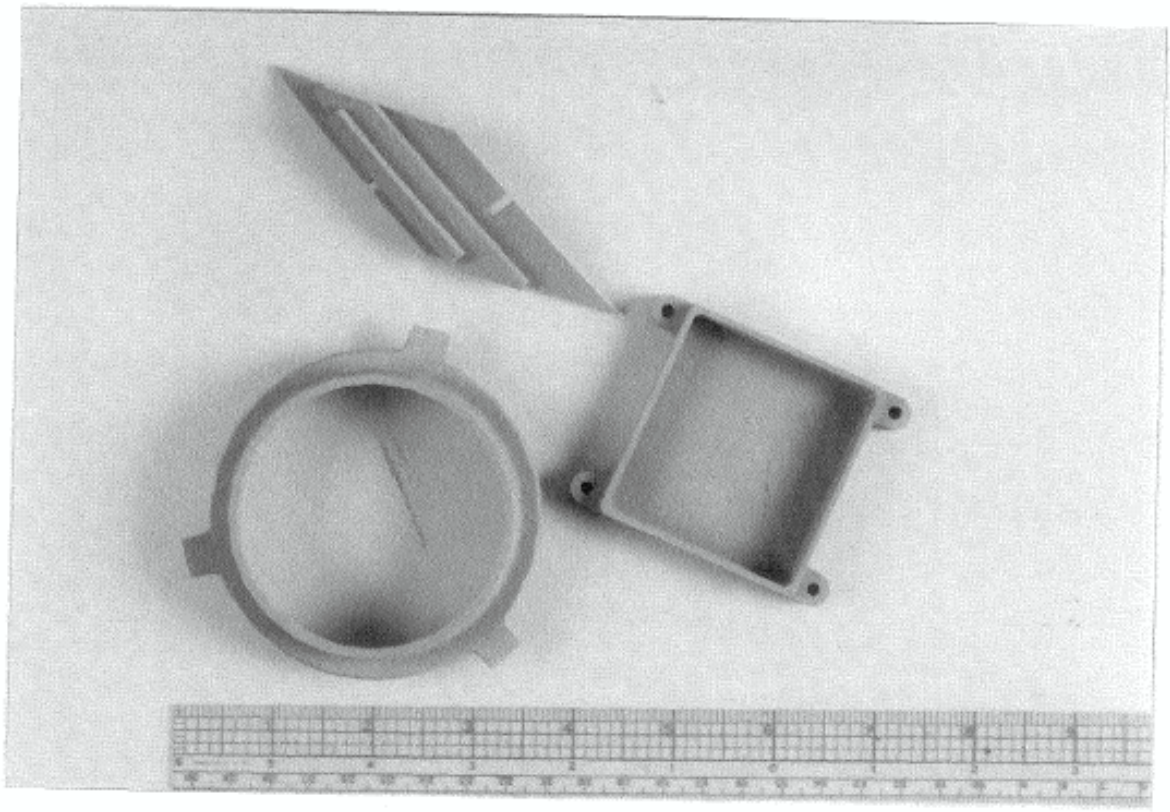

Figure 11. Silicon carbide preforms.

This research was supported by DARPA/ONR grant N000 14-92-J-1394 and DARPA grant MDA 972-92-J-1026 through Lanxide Corporation. DTM Corporation made available the SLS™ Model 125 workstation for these studies. Appreciation is given to Mike Durham, of the Austin Service Bureau, for his cooperation in obtaining experiment time on the workstation.

References

1. N.K. Vail and J.W. Barlow, *Solid Freeform Fabrication Symposium Proceedings*, **1**, 1 (1990).

2. B. Badrinarayan and J.W. Barlow, *Solid Freeform Fabrication Symposium Proceedings*, **3**, 141 (1992).

3. N.K. Vail and J.W. Barlow, *Solid Freeform Fabrication Symposium Proceedings*, **2**, 195 (1991).

4. N.K. Vail and J.W. Barlow, *ibid,* ref 2, p. 124.

5. B.W. Sorenson, G.H. Schiroky, and A.W. Urquhart, *Turbomachinery International,* **[9]** (1990).

6. A.W. Urquhart, *Advanced Materials and Processes,* **[7]** (1991).

7. S. Ashley, *Mechanical Engineering,* **[7]** (1991).

8. N.K. Vail and J.W. Barlow, "Development of a Poly(methyl methacrylate - co - *n*-butyl methacrylate) Copolymer Binder System", *in press.*

9. J.C. Nelson, Ph.D. Dissertation, The University of Texas at Austin, 1993.

10. U. Lakshminarayan, Ph.D. Dissertation, The University of Texas at Austin, 1992.

11. M. Yu. Bal'shin, Doklady Akademi Science, USSR, **67** [5], 831.

12. U. Lakshminarayan, Ph.D., DTM Corporation, *Private Communication.*